

Investigating the importance of social vulnerability in opioid-related mortality across the United States

Andrew J. Deas^{1,2,*}, Adam Spannaus², Dakotah D. Maguire², Jodie Trafton³, Anuj J. Kapadia²,
and Vasileios Maroulas^{1,*}

Author Affiliations:

¹Department of Mathematics, University of Tennessee, Circle Dr, Knoxville, 37916, TN, USA

²Computational Sciences and Engineering Division, Oak Ridge National Laboratory, Bethel Valley Road, Oak Ridge, 37830, TN, USA

³Office of Mental Health, Veterans Health Administration, Willow Road, Palo Alto, 94025, CA, USA

*Corresponding authors:

Andrew J. Deas

1 Bethel Valley Road, Oak Ridge, TN 37830

deasaj@ornl.gov

Vasileios Maroulas

Ayres Hall, 1403 Circle Dr, Knoxville, TN 37916

vmaroula@utk.edu

Classification: Research Report

Keywords: machine learning, data analysis, anomaly analysis, opioid crisis, XGBoost, autoencoder

Included in this pdf file: main text, figures 1 through 7, tables 1 and 2

Abstract

The opioid crisis remains a critical public health challenge in the United States. Despite national efforts to reduce opioid prescribing rates by nearly 45% between 2011 and 2021, opioid overdose deaths more than tripled during this same period. This alarming trend reflects a major shift in the crisis, with illegal opioids now driving the majority of overdose deaths instead of prescription opioids. Although much attention has been given to supply-side factors fueling this transition, the underlying socioeconomic conditions that perpetuate and exacerbate opioid misuse remain less understood. Moreover, the COVID-19 pandemic intensified the opioid crisis through widespread social isolation and record-high unemployment; consequently, understanding the socioeconomic drivers of this epidemic has become even more crucial in recent years. To address this need, our study examines the correlation between opioid-related mortality and thirteen components of the Social Vulnerability Index (SVI). Leveraging a nationwide county-level dataset spanning consecutive years from 2010 to 2022, this study integrates empirical insights from exploratory data analysis with feature importance metrics derived from machine learning models. Our findings highlight critical social factors strongly correlated with opioid-related mortality, emphasizing their potential roles in worsening the epidemic when their levels are high and mitigating it when their levels are low.

Abstract word count: 201

Significance Statement:

The opioid crisis remains one of the most pressing public health challenges in the United States, with overdose deaths more than tripling between 2011 and 2021 despite significant reductions in opioid prescribing. This study addresses a critical gap in understanding the socioeconomic factors that exacerbate or mitigate the crisis by leveraging a nationwide county-level dataset spanning over a decade. Integrating data analysis with machine learning, this study identifies key social factors that are strongly correlated with opioid-related mortality. Our findings provide actionable insights to inform interventions aimed at reducing opioid-related mortality across the nation.

Significance statement word count: 94

Introduction

The opioid crisis in the United States remains one of the most daunting and complex public health challenges in recent history. Initially driven by prescription practices, national efforts and legislation to decrease the availability of opioids have significantly reduced prescriptions from 257.9 million in 2011 to 143.4 million in 2020, a 44.4% decrease [1–3]. This decline in prescriptions has not led to a corresponding reduction in opioid-related overdose deaths however. On the contrary, opioid overdose death rates have surged within this same period [4]. In 2011, the rate stood at 7.3 per 100,000 persons, but by 2021, it had more than tripled to 24.7 per 100,000 persons [5].

These unsettling trends highlight a critical transformation in the opioid epidemic: Misuse is no longer primarily sustained through prescription medications but has shifted to illicit opioids such as fentanyl, methamphetamine, and heroin [6,7]. This transition has been driven by several factors, including the increased availability of low-cost, high-potency synthetic opioids [8,9], the widespread mixing of drugs with unpredictable potency [10–12], the proliferation of online platforms enabling the distribution of illegal substances [13,14], and worsening socioeconomic conditions linked to “deaths of despair” [15–17]. Although these factors had been exacerbating the epidemic well before 2020, the social isolation and record-high unemployment levels caused by the COVID-19 pandemic have further intensified the crisis [18–22].

While much attention has been given to the supply-side factors driving the opioid crisis, the underlying socioeconomic conditions that perpetuate and worsen opioid misuse are not as well understood. A growing body of research suggests that elements of the Social Vulnerability Index (SVI)—a composite measure designed to capture a community’s resilience to external stressors—play critical roles in shaping opioid-related outcomes [23–25]. For instance, social vulnerability factors have been identified as reliable predictors of opioid-related mortality [26], counties with higher social vulnerability rates tend to exhibit greater rates of opioid use disorder (OUD) [27], and communities with greater vulnerability due to housing type or lack of transportation have reduced access to medications for OUD [25].

While previous studies have provided important insights into the relationship between social vulnerability and opioid-related mortality, significant limitations persist. Many rely on cross-sectional data that does not capture trends over consecutive years and focus on aggregate SVI measures rather than its individual components. To address these gaps, this study utilizes a nationwide county-level dataset spanning consecutive years from 2010 to 2022 to examine the correlations between thirteen individual components of the SVI and opioid-related mortality. Mortality data were sourced from the CDC WONDER database, which included many suppressed values. To overcome this limitation, we developed an effective imputation method to ensure a more complete and accurate analysis of the relationships between SVI components and opioid-related mortality.

To identify which SVI components are most strongly correlated with opioid-related mortality, we leverage insights from exploratory data analysis alongside feature importance results derived from machine learning models. While machine learning excels at identifying predictive variables, its results can sometimes highlight relationships that are not meaningful in real-world contexts. Conversely, data analysis uncovers empirical relationships but may fall short in predictive ability. Integrating these two methods allows us to address the limitations of each and gain a more comprehensive understanding.

We begin this study by examining how the rates of each SVI component manifest in counties with anomalously high and low mortality rates. By identifying variables that exhibit their highest levels in high-mortality counties and their lowest levels in low-mortality counties, we highlight factors with bidirectional impacts across the mortality spectrum. Building on these empirical results, we then identify which SVI components are key contributors to opioid-related mortality predictions using feature importance metrics from two machine learning models.

The first model, XGBoost, is a decision tree-based algorithm with a proven track record in classification and regression tasks across various domains [28–31]. It evaluates feature importance using information gain, which measures how much each feature improves predictive accuracy when splitting a decision tree node. The second model, an augmented autoencoder, compresses input data into a lower-dimensional latent space and reconstructs it to predict mortality rates [32–34]. To tailor the architecture for this study, the autoencoder was augmented with a preliminary convolutional layer to aggregate the SVI components. To quantify each feature’s importance in the autoencoder, we utilized a Shapley Gradient Explainer, which identifies the variables that most significantly influence predictions when perturbed [35–37].

By integrating these complementary approaches, this study advances the understanding of the complex relationships between social vulnerability and opioid-related mortality. Our findings reveal critical socioeconomic factors that are strongly correlated with opioid-related mortality, highlighting variables that may exacerbate the epidemic at high levels and mitigate it at low levels. These insights offer a valuable foundation for designing public health interventions aimed at addressing the ongoing opioid crisis.

Results

Data analysis

We sourced mortality rates from the Centers for Disease Control and Prevention’s Wide-ranging ONline Data for Epidemiologic Research (CDC WONDER) system [38], which suppresses death counts in counties with fewer than 10 deaths. Consequently, mortality rates were unavailable for nearly half of the nation’s counties in each year of the study period. To address this data censoring,

we developed an effective methodology to impute missing values based on data from neighboring counties, as detailed in the Materials and Methods section.

Using this imputed dataset, our study begins by analyzing how the rates of each SVI component manifest in counties with anomalous mortality rates. In brief, each year we define anomalies as rates that fall within specific probabilities of a statistical distribution fitted to the nonzero mortality rates. Zero values were excluded because they make up a significant portion of the data, up to 947 counties, or 30.12% of the data in some years; they therefore do not represent anomalous cases. Consequently, the set of possible fitted distributions is restricted to those defined over the range $(0, \infty)$.

To determine the best-fitting distribution, we evaluated Gamma, Weibull, inverse Gaussian, and lognormal distributions. The goodness-of-fit was assessed using the Kolmogorov-Smirnov test, Akaike Information Criterion, and Bayesian Information Criterion. Based on these statistical measures, the lognormal distribution consistently outperformed the other candidates, scoring as the best-fitting distribution each and every year in the study period. Using these fitted distributions, anomalies are defined annually in two categories as follows: “Hot anomalies” are counties with nonzero rates above the 98th percentile of the yearly fitted distribution, while “cold anomalies” are those whose nonzero rates fall below the 2nd percentile. To select the size of these tails, we assessed 1%, 2%, and 3% thresholds. In some years, a 1% tail produced no cold anomalies, whereas the 2% tail always provided them. While a 3% tail also could have been used, to maximize the anomalous nature of the rates, we opted for the tightest bounds that still yielded cold anomalies for analysis each year. Figure 1 shows how the anomalies in 2016 change with 1%, 2%, and 3% tails.

To compare the rates of each SVI component within the anomalous counties, we rank the variables based on their mean rates. Specifically, we first calculate the mean rate within each year and then average these yearly means over the entire study period. Features are ordered from highest to lowest average mean rate in hot counties and from lowest to highest in cold counties. These rankings identify the variables most strongly correlated with anomalous mortality rates. The results are presented in figure 2, where yearly mean rates for each feature are shown using colored bars, and black bars indicate each variable’s average mean rate across all years of the study.

Figure 2a ranks the SVI variables based on their average mean rates in the hot counties. Among these hot counties, the component with the highest average mean rate is no vehicle (75.40), followed by below poverty (75.22), no high school diploma (73.48), unemployment (70.18), and mobile homes (68.61). The high ranking of these features means they tend to manifest their highest rates in counties with anomalously high opioid-related mortality. This suggests that opioid-related mortality may be exacerbated by high levels of these factors. Beyond these top five, rates noticeably decline, starting with single-parent households (54.61) and continuing to drop further down the list. At the bottom are limited English ability and minority status, meaning they have the lowest average rates in the hot counties. This suggests that these components may contribute the least to the

exceptionally high mortality rates observed in the hot counties.

Figure 2b ranks the SVI variables based on their average mean rates in the cold counties. Among these cold counties, the component with the lowest average mean rate is unemployment (35.58), followed by multi-unit structures (39.66), single-parent households (39.89), limited English ability (42.22), and no vehicle (42.84). The high ranking of these features means they tend to manifest their lowest rates in counties with anomalously low opioid-related mortality. This suggests that opioid-related mortality may be alleviated by lower levels of these factors. Beyond these top five, mean rates only gradually increase, except at the bottom, where a significant jump is observed for the variable aged 65 or older. This factor stands out with the highest average mean rate (61.74) in the cold anomalies, indicating that counties with anomalously low opioid-related mortality tend to have a significantly higher population of persons aged 65 or older.

Notably, only two components—unemployment and lack of vehicle access—exhibited bidirectional relationships, with their highest rates occurring in counties with anomalously high mortality and their lowest rates in counties with anomalously low mortality. The fact that these variables are observed at both extreme ends of the mortality rate spectrum suggests that they may play a particularly significant role: High levels may contribute to increased opioid-related mortality, while low levels may help reduce it. These empirical results provide a real-world foundation for the subsequent machine learning analysis, identifying which SVI features are the key contributors to opioid-related mortality predictions.

Efficacy of machine learning models

This study employed two machine learning models to predict opioid-related mortality rates from 2011 to 2022 using the previous year’s SVI data. XGBoost generates predictions for each county by combining the outputs from an ensemble of decision trees, where each tree iteratively corrects the errors of its predecessors through gradient-based optimization. The autoencoder model, on the other hand, processes input data through an initial 1D convolutional layer that aggregates SVI variables before passing the data to an encoder, which compresses it into a lower-dimensional representation. This representation is then decoded to produce the yearly mortality rate predictions.

The efficacy of our machine learning models in forecasting county-level mortality rates is evaluated using both accuracy and error metrics. For each county, the error is measured as the absolute residual. To assess overall accuracy, the maximum absolute residual, which indicates the largest annual prediction error, is used as a benchmark: Each county’s error is normalized by this highest observed error across the country. The performance of the models is summarized in table 2, which presents the average errors, maximum errors, and average accuracy of both models for each predictive year in the study period. While each year is treated as an independent test year by XGBoost, 2022 serves as the sole testing year for the autoencoder. This approach was chosen to preserve

the natural temporal trajectory of the opioid crisis by training the autoencoder sequentially on data from 2010 to 2020, with 2021 as the testing year and predictions made for 2022. Accordingly, we present visual representations of the 2022 efficacy results using error histograms (fig. 3) and accuracy maps (fig. 4).

As seen in table 2, both models generally maintain high accuracy throughout the study period, yet exhibit a notable increase in average and maximum errors starting in 2020 which persist through 2022. Some of these errors could be attributable to problems inherent in data censoring. The maximum error for both models in 2022 arises in Menominee County, Wisconsin, where the 2021 mortality rate was censored and subsequently imputed using our method. This imputation, based on neighboring counties, produced a value of 26.16; yet, the reported rate for 2022 was 238.27—a 810.82% increase that neither model could predict. This extreme increase could be attributed to a reporting error in either 2021 or 2022, or to the low imputed value from the previous year due to the censored data in that year. Not all large errors might be attributable to data censoring however. For example, the second largest error in 2022 for both models occurs in Bath County, Kentucky. This county reported a mortality rate of 86.09 in 2021, which nearly doubled to 163.69 in 2022—a 90.14% increase from the previous year that both models struggled to predict. The errors stemming from Menominee and Bath counties are highlighted in fig. 3, which displays the complete 2022 error distributions for both models, providing a visual comparison of their error ranges.

Figure 4 shows each model’s 2022 accuracy maps, both characterized predominantly by green hues, reflecting high predictive accuracy nationwide. Menominee County, Wisconsin, which had the largest 2022 error for both models, is marked correspondingly in the darkest shade of red. While Bath County, Kentucky, appears in orange on the autoencoder’s accuracy map and in yellow on XGBoost’s map. This discrepancy is due to the sharp increase in mortality rates in Bath County from 2021 to 2022, which contributed to a larger error for the autoencoder than XGBoost in that year.

XGBoost feature importance

We used XGBoost to predict opioid-related mortality rates from 2011 to 2022 based on the previous year’s SVI data. To assess the importance of each SVI component, XGboost utilizes information gain:

$$G(Q_n, \theta) = L(Q_n) - \left(\frac{s_n^{left}}{s_n} L(Q_n^{left}(\theta)) + \frac{s_n^{right}}{s_n} L(Q_n^{right}(\theta)) \right).$$

This metric, detailed in the materials and methods section, quantifies the improvement in the model’s predictive performance when a feature is used to split a node in a decision tree. As a result, the features with the highest gain scores are those that most significantly improve the model’s

ability to predict opioid-related mortality rates.

The feature importance results for XGBoost are displayed in fig. 5a. In this image, each feature’s yearly importance scores are shown with colored bars, while each feature’s average importance score across the entire study period is represented by the black bars. These black bars rank the components from highest average importance down to lowest.

Significantly surpassing all others, unemployment (0.1585) has the highest average importance score. This is followed by minority status (0.0814), but its average importance score is only slightly over half that of unemployment. While its yearly importance scores fluctuate slightly, unemployment occupies the top spot every year. As we move further down the list, feature importance scores only continue to decrease. Notably, the dominant role unemployment plays in predicting opioid-related mortality rates for XGBoost corroborates the empirical findings of the data analysis.

Autoencoder feature importance

In this study, the autoencoder model was used to predict opioid-related mortality rates from 2011 to 2022 based on the previous year’s SVI data. To determine which components of the SVI were most important in the autoencoder’s predictions, we applied a Shapley Gradient Explainer to the initial convolutional layer. The Shapley Gradient Explainer generates SHAP (Shapley Additive Explanations) values, which quantify the contribution of each feature to a model’s predictions [35–37]. By measuring how sensitive the autoencoder’s mortality predictions are to small changes in each feature, the SHAP values identify the most important components as those for which minor changes lead to the greatest impact on predictions.

The feature importance results for the autoencoder are showcased in Figure 5b. In this image, each feature’s yearly SHAP value is shown with colored bars, while each feature’s average SHAP value across the entire study period is represented by the black bars. These black bars rank the components from highest average importance down to lowest.

The variable with the highest average SHAP value is crowding (0.00143), followed closely by no vehicle (0.00137) and multi-unit structures (0.00136). In fourth place is aged 65 or older (0.00131), from which SHAP values gradually decrease down to unemployment (0.00116) in seventh place. Beyond unemployment, there is a noticeable drop in the SHAP values for mobile homes and minority status. After which, there is another steep decline in importance moving down to the the last four components. This reflects the much smaller contribution these four factors make to the model’s predictions. Notably, the high importance score of no vehicle corroborates the empirical findings from the data analysis.

SHAP values are relative to the model, data, and problem context; they reflect the contributions of each feature to the predictions compared to the baseline (i.e., the average prediction). Ranking these values within the model provides a reliable and interpretable measure of feature importance,

offering meaningful insights into the influence of each component on this specific model and dataset.

Discussion

Utilizing thirteen components of the SVI, this study sought to identify which variables are most strongly correlated with opioid-related mortality. The data analysis portion of this study examined how the rates of each component manifested in counties with anomalous mortality. Notably only two factors—unemployment and lack of vehicle access—exhibited bidirectional relationships, with their highest rates observed in counties with anomalously high mortality and their lowest rates in counties with anomalously low mortality. This pattern suggests that reducing unemployment and improving vehicle access may lead to measurable reductions in opioid-related mortality, particularly in the most severely affected regions.

These empirical results provided real-world grounding for the subsequent machine learning analysis, which identified the SVI components that are key contributors to opioid-related mortality predictions. This portion of the study employed two machine learning models: XGBoost and an autoencoder. Feature importance was assessed using information gain for XGBoost and a Shapley gradient explainer for the autoencoder. While the feature importance rankings differed between the two models, this difference highlights the value of employing multiple approaches, as it revealed critical insights that might have been overlooked if only one model had been used.

In the XGBoost model, unemployment emerged as the most important feature by a significant margin; the second-ranked feature, minority status, had an importance score just over half that of unemployment. This indicates that unemployment is nearly twice as strong a predictor of opioid-related mortality than any other variable in the XGBoost model. Although crowding ranked highest in the Shapley analysis of the autoencoder, lack of vehicle access followed closely in second place with a nearly identical importance score. This indicates that small changes in vehicle access rates produced substantial shifts in the autoencoder’s mortality predictions. These results from the machine learning analysis corroborate those from the data analysis; they underscore unemployment and lack of vehicle access as strongly correlated with opioid-related mortality and highlight their potential roles as key factors in the opioid epidemic.

By quantifying the contribution of unemployment to opioid-related mortality predictions using feature importance metrics from two machine learning models, this analysis builds on the well-established connection between unemployment and opioid-related outcomes [39–41]. Previous work has shown that unemployment, along with the accompanying economic hardships, significantly contributes to opioid misuse in the United States [42–44]. These studies emphasize the importance of employment-related factors in addressing the opioid crisis, and call for substance abuse treatment to remain a priority even during economic downturns. Beyond economic strain, unemployment has

been shown to disrupt the structure, routine, social connections, and sense of identity that are critical to recovery for individuals with OUD [45].

Although transportation barriers have been recognized as significant obstacles to general health-care access in prior research [46–49], the role of household vehicle ownership in the opioid crisis remains largely underexplored. Lack of a household vehicle can lead to missed or delayed healthcare appointments, increased health expenditures, and poorer health outcomes [50]. These issues are particularly significant in the daily life of individuals struggling with OUD. In opioid-related emergencies, such as overdoses, direct access to transportation becomes vital, as the lack of it can delay life-saving care. Additionally, many underserved communities facing opioid challenges often lack adequate transportation, forcing individuals without vehicles to rely on limited local resources [46,51]. For example, research has documented an alarming rise in opioid-related overdose deaths within Black urban populations, partly attributing this trend to the lack of available transportation in these communities [52].

In addition to highlighting the importance of unemployment and lack of vehicle access in opioid-related mortality, this study also underscores the detrimental impact of the COVID-19 pandemic on the national opioid crisis. While this impact has been previously discussed [18,53,54], our work adds to the conversation by providing novel support. This is seen in the performance of our models, where we observe a notable increase in errors beginning in 2020 and persisting through 2022. This trend is significant because the autoencoder retains learned temporal patterns, whereas XGBoost treats each year of data independently without learning across time. The fact that both models exhibit similar error patterns during this period suggests that the opioid crisis worsened during the pandemic to such a degree that previous data patterns no longer provided useful predictive insights for the autoencoder.

The intensifying effects of the COVID-19 pandemic on the national opioid crisis were driven in part by two key factors: social isolation and unemployment [19–22]. Unemployment in the United States surged to unprecedented levels during the pandemic, peaking at 14.8% in April 2020 and gradually declining to 6.2% in February 2021, still well above the pre-pandemic rate of 3.6% in 2019 [55]. Additionally, the social isolation caused by pandemic lockdowns was shown to have detrimental effects on mental health and substance use outcomes [21,22]. This social isolation, experienced widely during the pandemic, might reflect a similar form of isolation faced by individuals without access to reliable transportation, particularly in rural regions where public transit is limited and community resources are spread out. In this way, the COVID-19 pandemic highlights the destructive impact that both unemployment and lack of vehicle access can have on the national opioid crisis.

Public health interventions could mitigate these impacts by prioritizing strategies that address both economic stability and transportation access. Workforce development programs that focus

on providing stable, meaningful employment opportunities could play a critical role in reducing the socioeconomic stressors that contribute to opioid misuse, particularly in regions with high opioid-related mortality. Additionally, improving access to reliable and affordable transportation, especially in underserved communities and rural regions, could help alleviate the barriers faced by those without personal vehicles. By addressing these fundamental social vulnerabilities, targeted interventions could help reduce the impact of these two critical factors and may even promote long-term recovery in the nation’s most vulnerable areas.

This study has important limitations to note, beginning with the issue of missing mortality data in the CDC WONDER dataset. Although we employed methods to address this, no approach can fully overcome the challenges posed by suppressed data. This limitation was sometimes evident when real data, missing in the previous year, became available the following year at a much higher rate than the previously imputed value. This sharp increase sometimes led to large predictive errors in both models. Future research could apply the methodologies outlined in this study to a dataset with fewer missing values, if such data is available.

The next limitation to note is that this study does not stratify counties by urban or rural designation; there are stark differences in how vehicle access impacts opioid-related mortality within these two contexts. In urban areas, such as New York City, low vehicle ownership rates are often offset by robust public transportation systems, making personal vehicles less essential for accessing healthcare. Conversely, in rural regions, such as those in Appalachia, lacking a vehicle often equates to extreme isolation, severely limiting access to medical services and treatment. Future studies could explore such urban-rural dynamics to develop context-specific strategies that address transportation barriers in a manner tailored to local needs.

Finally, the opioid crisis is a highly complex issue, influenced by many factors beyond those considered in this study. Future work could expand on the methodologies used here by investigating a broader range of factors contributing to opioid-related mortality.

Materials and Methods

Mortality data

This study utilizes county-level opioid-related mortality rates, measured per 100,000 persons, from 2010 to 2022. Throughout the study period, the county structure of the United States changed due to the formation of new counties and the reconfiguration of existing ones [56]. For example, Connecticut completely restructured its county boundaries in 2022 [57]. Such changes impacted data consistency across years. Also, the machine learning models used in this study require a fixed input dimension; therefore the data has been curated to reflect the 2022 county structure, which includes 3,144 counties. This step ensures that we provide the most up-to-date and cohesive

representation of the national county landscape with respect to the data.

This mortality data was sourced from the CDC WONDER online database. The data were pulled using underlying cause-of-death codes from the Tenth Revision of ICD (ICD-10): X40–X44 (unintentional), X60–X64 (suicide), X85 (homicide), and Y10–Y14 (undetermined) [58, 59]. It is therefore important to note that these rates serve as indicators of opioid misuse rather than exact counts of opioid overdose mortality. These data were retrieved at the county level, with the specified ICD-10 codes, while the other categories were left in their default settings.

Method for handling missing data

The CDC WONDER database suppresses death counts in counties with fewer than 10 deaths. As a result, many mortality rates were missing, about half the nation’s counties in each year of the study period. Thus to use this data in our study, it was essential to develop an effective methodology for imputing the missing values. One approach used in a previous study involved imputing missing death rates utilizing available data from neighboring counties [60]. In their method, each county’s neighborhood was defined as the entire state in which that county resides. In this study, we adopt a similar approach but use a more localized strategy: We impute missing mortality rates by averaging the available rates from a county’s queen adjacent neighbors—counties that share a direct border or a corner.

Utilizing the queen adjacent counties, our methodology proceeds in a step-wise manner. First, rates for counties with exactly one missing neighbor are imputed by averaging the available neighboring county rates. Next, counties with two missing neighbors are addressed in the same way, followed by those with three missing neighbors. This process repeats iteratively until only counties for which all neighbors have available data remain. These counties are handled at the end because they do not impact the earlier steps, and their missing rates are imputed by averaging over the full set of neighboring counties.

Next, we address island counties with missing data. These counties are geographically separated from the mainland and therefore lack queen adjacent neighbors. For these island counties, which number at most three in any given year, we construct neighborhoods using the closest continental neighbors. Missing rates are then imputed by averaging rates over these constructed continental neighborhoods.

Our approach focuses exclusively on imputing mortality rates rather than raw death counts. This distinction is critical because mortality rates are calculated relative to a county’s population; small changes in raw death counts can lead to disproportionately large shifts in mortality rates, particularly in counties with small populations. Imputing raw death counts could introduce significant variability and potentially distort the derived rates, undermining the reliability of the imputation. By focusing directly on the mortality rates, our approach minimizes sensitivity to population size

and ensures more consistency in the data.

To demonstrate the effectiveness of our methodology, we present national mortality rate maps for 2013. This year had the most significant data censoring, with 1,681 out of 3,144 counties lacking mortality rates, or 53.47% of the data. Figure 6 displays maps both with and without the missing data, each colored by percentiles from the respective empirical distributions. Figure 6a illustrates the extent of the missing data, revealing an incomplete view of national mortality rates. In contrast, Figure 6b shows the results after applying our imputation method; previously missing regions are now filled with interpolated data that preserves the spatial patterns of the original dataset. This significant improvement highlights the effectiveness of our approach, allowing us to address substantial data gaps and create a more complete and accurate national dataset for analysis.

Finally, Connecticut’s county structure underwent a complete change in 2022. Since our dataset is curated to reflect the 2022 county boundaries, we needed to account for this structural change in all prior years of the study. To do this, we used the Python package Tobler [61], which specializes in spatial interpolation. Tobler allowed us to transfer data from the old county boundaries (2010 to 2021) to the new 2022 structure by interpolating mortality rates between the two geographic frameworks. This interpolation adjusts for differences in county areas, and ensures that population-dependent variables like mortality rates are accurately represented in the new structure.

Figure 7 demonstrates the results of using the Tobler library to interpolate mortality rates for Connecticut in 2021, the last year before the county structure changed. Figure 7a displays Connecticut’s old county structure (pre-2022), while Figure 7b shows the new 2022 boundaries. For direct comparison, the color scales for both maps are normalized to the minimum and maximum 2021 mortality rates across both county structures. As an example, counties 09003 and 09013 from the old structure roughly correspond to county 09110 in the new 2022 structure. Here the interpolated data accurately reflects this consolidation, with the interpolated value being substantially larger than both old values. For another example, county 09009 in the old structure roughly corresponds to counties 09140 and 09170 in the new structure. In this example, the interpolated data captures this division effectively, with both interpolated values considerably lower than the old value.

SVI data

This study uses county-level rank ordered percentile estimates (ranging from 0 to 100) of thirteen components of the SVI across the United States from 2010 to 2022. The set of SVI variables utilized for 2010 data collection differs from those used in 2022. Therefore, we were forced to exclude all variables that were not available across every year in the study period, resulting in the thirteen SVI features utilized in this study. All data were sourced from the CDC and the Agency for Toxic Substances and Disease Registry’s Social Vulnerability Index, which utilizes data from the American Community Survey to assess the resilience of communities to external stresses on human health [23].

The 2010 SVI data was not followed by another release until 2014, after which the data has been released biennially. To account for the gap between 2010 and 2014, we imputed the intervening years by calculating a quarter of the difference between the 2010 and 2014 data points and adding it consecutively to each year starting in 2014. After 2014, for the biennial data releases, we applied a similar method by calculating half the difference between consecutive data points and adding it to the earlier year’s rates. This method, with the understanding that yearly rate fluctuations are modest, provided a viable way to analyze the impact of these social vulnerability factors on the national opioid crisis throughout the entire study period.

Notably, Rio Arriba County, New Mexico, experienced a data collection error in 2018, resulting in a suppressed value for that year [62]. Therefore, in this situation, we applied the same approach used for the gap between 2010 and 2014, taking a quarter of the difference between the 2016 and 2020 data points and adding it consecutively to each year starting in 2016. Overall, the SVI data had minimal missing values, at most four counties in any given year of the study. These missing rates were imputed using the exact same methodology employed for the mortality rates.

XGBoost model

In this study, XGBoost was used to predict opioid-related mortality rates from 2011 to 2022 based on the previous year’s SVI data. To use XGBoost, several parameters need to be selected, such as the number and depth of trees. To select these parameters, we employed a grid search algorithm with cross-validation, optimizing for the highest predictive accuracy. For training and testing, we used 5-fold cross-validation to randomly split the SVI input data into five folds. In each fold, XGBoost trained on four subsets and predicted on one. This process was repeated across all five folds to generate predictions for every county, ensuring that the model was both trained and tested on the entire SVI dataset.

To describe this model mathematically, fix a year $t \in \{2010, 2011, \dots, 2021\}$ and let $X^{(t)} = [x_{i,j}^{(t)}] \in \mathbb{R}^{3144 \times 13}$ be the matrix of SVI features input to the model in year t . Each row of matrix $X^{(t)}$ corresponds to a county, while each column corresponds to an SVI variable. In particular, let $x_{i,*}^{(t)}$ denote the row vector containing all the SVI feature data for county i , and let $x_{*,j}^{(t)}$ denote the column vector containing all county rates for SVI variable j . Letting $Y^{(t+1)} = (y_i^{(t+1)}) \in \mathbb{R}^{3144}$ be the target vector of mortality rates in year $t + 1$, we can define the full dataset $X^{(t)} \times Y^{(t+1)}$ passing through the model to be the set of all counties’ feature vectors together with their corresponding target values:

$$X^{(t)} \times Y^{(t+1)} = \{(x_{i,*}^{(t)}, y_i^{(t+1)}) \mid i \in \{1, 2, \dots, 3144\}\}$$

Starting with the root node, an individual decision tree grows by recursively applying a splitting

process to each node n in the tree. Let the data at node n be denoted by Q_n with s_n samples. Then s_n is the number of counties which reached that node, and $Q_n \subseteq X^{(t)} \times Y^{(t+1)}$ is the subset of data for those counties. At each node, a potential split $\theta = (j, h_n)$, consisting of an SVI feature j and a threshold h_n , partition Q_n into two subsets:

$$\begin{aligned} Q_n^{left}(\theta) &= \{(x_{i,*}^{(t)}, y_i^{(t+1)}) \mid x_{i,j}^{(t)} \leq h_n\}, \\ Q_n^{right}(\theta) &= Q_n \setminus Q_n^{left}(\theta). \end{aligned}$$

$Q_n^{left}(\theta)$ is the data for counties satisfying the boolean condition of the split, meaning these data points proceed down the tree's left path; while $Q_n^{right}(\theta)$ contains the data for counties which did not satisfy the split condition, meaning these data points proceed down the right path. The quality of a potential split at node n is measured using a loss function $L(Q)$ which evaluates how well the data in an arbitrary set Q fits the target values. In particular, we utilize the mean absolute error as the loss function:

$$L(Q) = \frac{1}{|Q|} \sum_{(x_{i,*}^{(t)}, y_i^{(t+1)}) \in Q} |y_i^{(t+1)} - \hat{y}_i^{(t+1)}|,$$

where $|Q|$ represents the total number of elements in the set Q , and $\hat{y}_i^{(t+1)}$ is the predicted mortality rate for county i .

The gain $G(Q_n, \theta)$ from splitting Q_n by θ is then given by

$$G(Q_n, \theta) = L(Q_n) - \left(\frac{s_n^{left}}{s_n} L(Q_n^{left}(\theta)) + \frac{s_n^{right}}{s_n} L(Q_n^{right}(\theta)) \right). \quad (1)$$

Here s_n^{left} is the number of counties which satisfied the split condition, and s_n^{right} is the number that did not. The optimal split $\tilde{\theta}$ at this node is then chosen by maximizing the gain:

$$\tilde{\theta} = \operatorname{argmax}_{\theta} G(Q_n, \theta). \quad (2)$$

This process creates child nodes from the subsets $Q_n^{left}(\tilde{\theta})$ and $Q_n^{right}(\tilde{\theta})$. It continues recursively until a stopping criterion is met, such as reaching the minimum number of samples at a node or when no further improvement in gain is possible. Mortality rate predictions are then made at these nodes with no further splits, called leaf nodes or terminal nodes. If n is a terminal node, then the prediction for each county i which reached this node is

$$\hat{y}_i^{(t+1)} = \frac{1}{s_n} \sum_{(x_{i,*}^{(t)}, y_i^{(t+1)}) \in Q_n} y_i^{(t+1)}.$$

To evaluate the importance of each SVI component in the model, XGBoost utilizes the gain from eq. (1). This metric reflects the improvement in the model’s predictive performance when an SVI feature is used to split a decision node. At each node, the optimal split was chosen via eq. (2), which can be rewritten as follows:

$$(\tilde{j}, \tilde{h}_n) = \operatorname{argmax}_{j, h_n} G(Q_n, (j, h_n)). \quad (3)$$

From eq. (3), we see that at each node, XGBoost evaluates all features $j \in \{1, 2, \dots, 13\}$ and selects the optimal feature \tilde{j} , along with a corresponding threshold, to maximize the gain.

As the decision trees are built, XGBoost sums the gains for each feature across all nodes and trees in the model. The total gain for feature j , denoted $G_{total}(j)$, is then the sum of the gains $G(Q_n, (\tilde{j}, \tilde{h}_n))$ over all nodes n in the model which split using feature j :

$$G_{total}(j) = \sum_{n=1}^J G(Q_n, (\tilde{j}, \tilde{h}_n)).$$

Here J is the number of nodes which used feature j to split. The features that contribute the most to improving the model’s predictive accuracy are those with the highest total gain. Consequently, SVI components with higher total gain are considered more important, as they most consistently reduce the prediction error across the model.

Autoencoder model

In this study, the autoencoder model was used to predict opioid-related mortality rates from 2011 to 2022 based on the previous year’s SVI data. The input data is first passed through the initial 1D convolutional layer, which aggregates the SVI variables before being fed into the encoder. The encoder compresses the data into a lower-dimensional representation, which is then passed to the decoder to produce the final vector containing yearly mortality rate predictions for each county in the nation.

To preserve the natural temporal structure of the opioid crisis, the model is trained sequentially on SVI data from 2010 to 2020, with 2015 held out as the validation set, and 2021 used for testing. To prevent overfitting, the model is allowed to train for up to 100 epochs, with early stopping triggered after 10 consecutive worse predictions on the validation set. The training process utilizes an L^1 loss function and a cyclical learning rate.

To describe the autoencoder model mathematically, again let $t \in \{2010, 2011, \dots, 2021\}$ denote a fixed year, and $X^{(t)}$ denote the input SVI data from year t . Let $\hat{Y}^{(t+1)}$ be the output vector of mortality rate predictions for year $t + 1$, and let A be the full neural network model. It consists of five layers: the initial 1D convolutional layer C , two encoding layers E_1 and E_2 , and two decoding

layers D_3 and D_4 . Then the model can be expressed as follows:

$$\begin{aligned}\hat{Y}^{(t+1)} &= A(X^{(t)}) \\ &= (D_4 \circ D_3 \circ E_2 \circ E_1 \circ C)(X^{(t)}).\end{aligned}$$

The convolutional layer C learns an effective way to convolve the thirteen SVI components, producing a single vector of size 3144. This vector represents the aggregate state of the nation with respect to the SVI variables. The convolutional layer can be written as:

$$C(X^{(t)}) = W_C \cdot X^{(t)} + b_C,$$

where W_C is the matrix of weights for this layer, and b_C is the vector of biases, both optimized through a stochastic gradient descent process.

The encoder layers E_1 and E_2 iteratively reduce the dimensionality of the input data. E_1 is followed by a ReLU activation function, while E_2 is not. For an arbitrary input x , these layers can be written as follows:

$$\begin{aligned}E_1(x) &= \text{ReLU}(W_{E_1} \cdot x + b_{E_1}), \\ E_2(x) &= W_{E_2} \cdot x + b_{E_2}.\end{aligned}$$

Here W_{E_i} and b_{E_i} are the weight matrices and bias vectors for $i \in \{1, 2\}$, respectively.

The decoder layers D_3 and D_4 then iteratively increase the dimensionality back to the original input space. For an arbitrary input x , these layers can be written as follows:

$$\begin{aligned}D_3(x) &= \text{ReLU}(W_{D_3} \cdot x + b_{D_3}) \\ D_4(x) &= W_{D_4} \cdot x + b_{D_4}.\end{aligned}$$

Here W_{D_i} and b_{D_i} are the weight matrices and bias vectors for $i \in \{3, 4\}$, respectively.

To gain insight into the most important features in the autoencoder’s mortality predictions, we employed a Shapley gradient explainer. This method, building on the concept of integrated gradients [36], utilizes the expected gradient approach to quantify the impact of each input feature [63]. Expected gradients are calculated by averaging the gradient of the model’s output with respect to each feature over the entire county structure, providing a measure of how each component impacts the autoencoder’s predictions. Each variable’s impact is quantified via a SHAP value [37], representing the contribution of that feature to the predicted mortality rates. Consequently, the most important features in the autoencoder model are those for which minor perturbations produce the greatest changes in the model’s output.

Acknowledgments

The authors would like to thank Heidi A. Hanson and Andrew Farrell for their helpful comments and feedback throughout the entire study.

Funding

This work is sponsored by the US Department of Veterans Affairs using resources from the Knowledge Discovery Infrastructure which is located at the Oak Ridge National Laboratory and supported by the Office of Science of the U.S. Department of Energy. This manuscript has been authored by UT-Battelle, LLC, under contract DE-AC05-00OR22725 with the US Department of Energy (DOE). The US government retains and the publisher, by accepting the article for publication, acknowledges that the US government retains a nonexclusive, paid-up, irrevocable, worldwide license to publish or reproduce the published form of this manuscript, or allow others to do so, for US government purposes. DOE will provide public access to these results of federally sponsored research in accordance with the DOE Public Access Plan (<http://energy.gov/downloads/doe-public-access-plan>)

Author contributions

AD conducted all core research activities, curated and analyzed the data, generated the code, and wrote the original manuscript. AS and VM supervised the research while providing general and methodological expertise. DM suggested the use of Tobler for interpolating data in Connecticut. All authors reviewed the manuscript and contributed to revisions.

Data availability

All datasets and code supporting this study are available in the ‘A-Deas/Opioid-Feature-Importance’ Github repository: <https://github.com/A-Deas/Opioid-Feature-Importance>.

Competing interests

The authors have no competing interests to declare.

References

- [1] CDC Overdose Prevention. Understanding the opioid overdose epidemic. <https://www.cdc.gov/overdose-prevention/about/understanding-the-opioid-overdose-epidemic.html>. Accessed August 1, 2024.

- [2] American Medical Association. Report shows decreases in opioid prescribing, increase in overdoses. <https://www.ama-assn.org/press-center/press-releases/report-shows-decreases-opioid-prescribing-increase-overdoses>. Accessed August 1, 2024.
- [3] National Institute on Drug Abuse. Prescription opioids and heroin research report. <https://nida.nih.gov/publications/research-reports/prescription-opioids-heroin/increased-drug-availability-associated-increased-use-overdose>. Accessed August 1, 2024.
- [4] Lucas Böttcher, Tom Chou, and Maria R. D’Orsogna. Forecasting drug-overdose mortality by age in the united states at the national and county levels. *PNAS Nexus*, 3(2):page050, 2024.
- [5] State Health Access Data Assistance Center. The opioid epidemic in the united states. <https://www.shadac.org/opioid-epidemic-united-states>. Accessed September 20, 2024.
- [6] National Academies of Sciences, Engineering, and Medicine, Jonathan K. Phillips, Morgan A. Ford, and Richard J. Bonnie. *Pain Management and the Opioid Epidemic: Balancing Societal and Individual Benefits and Risks of Prescription Opioid Use*. National Academies Press (US), Washington, DC, 2017. Available from: <https://www.ncbi.nlm.nih.gov/books/NBK458661/>.
- [7] Daniel Ciccarone. The rise of illicit fentanyl, stimulants and the fourth wave of the opioid overdose crisis. *Current Opinion in Psychiatry*, 34(4):344–350, Jul 2021.
- [8] Christopher M. Jones, Fadia Bekheet, Julia N. Park, and G. Caleb Alexander. The evolving overdose epidemic: Synthetic opioids and rising stimulant-related harms. *Epidemiologic Reviews*, 42(1):154–166, Jan 2020.
- [9] R. M. Krausz, J. N. Westenberg, N. Mathew, and T. Kerr. Shifting north american drug markets and challenges for the system of care. *International Journal of Mental Health Systems*, 15:86, 2021.
- [10] Mbabazi Kariisa, Jane O’Donnell, Sapna Kumar, Christine L. Mattson, and Bruce A. Goldberger. Illicitly manufactured fentanyl-involved overdose deaths with detected xylazine — United States, January 2019–June 2022. *MMWR Morbidity and Mortality Weekly Report*, 72:721–727, 2023.
- [11] Shoshana E. Duhart Clarke, Alex H. Kral, and Jon E. Zibbell. Consuming illicit opioids during a drug overdose epidemic: Illicit fentanyl, drug discernment, and the radical transformation of the illicit opioid market. *International Journal of Drug Policy*, 99:103467, Jan 2022.

- [12] Ashley Larnder, Armin Saatchi, Scott A. Borden, Belaid Moa, Chris G. Gill, Bruce Wallace, and Dennis Hore. Variability in the unregulated opioid market in the context of extreme rates of overdose. *Drug and Alcohol Dependence*, 235:109427, 2022.
- [13] Timothy K. Mackey. Opioids and the internet: Convergence of technology and policy to address the illicit online sales of opioids. *Health Services Insights*, 11:1178632918800995, Sep 2018.
- [14] Timothy Mackey, Janani Kalyanam, Joshua Klugman, Edward Kuzmenko, and Rishita Gupta. Solution to detect, classify, and report illicit online marketing and sales of controlled substances via twitter: Using machine learning and web forensics to combat digital opioid access. *Journal of Medical Internet Research*, 20(4):e10029, 2018.
- [15] Anne Case and Angus Deaton. Rising morbidity and mortality in midlife among white non-hispanic americans in the 21st century. *Proceedings of the National Academy of Sciences of the United States of America*, 112(49):15078–15083, Dec 2015.
- [16] Anne Case and Angus Deaton. Mortality and morbidity in the 21st century. *Brookings Papers on Economic Activity*, 2017(Spring):397–476, 2017.
- [17] Kasey Rehder, Joshua Lusk, and Jason I. Chen. Deaths of despair: Conceptual and clinical implications. *Cognitive and Behavioral Practice*, 28(1):40–52, Feb 2021.
- [18] Erin J. Stringfellow, Tse Yang Lim, Catherine DiGennaro, Zeynep Hasgul, and Mohammad S. Jalali. Enumerating contributions of fentanyl and other factors to the unprecedented 2020 rise in opioid overdose deaths: model-based analysis. *PNAS Nexus*, 2(4):pgad064, 2023.
- [19] Nicholas Morrish and Antonia Medina-Lara. Does unemployment lead to greater levels of loneliness? a systematic review. *Social Science & Medicine*, 287:114339, Oct 2021.
- [20] Francesco Bianchi, Giada Bianchi, and Dongho Song. The long-term impact of the covid-19 unemployment shock on life expectancy and mortality rates. *Journal of Economic Dynamics and Control*, 146:104581, 2023.
- [21] Erin L. Kelly, Megan K. Reed, Kathryn M. Schoenauer, Kelsey Smith, Kristina Scalia-Jackson, Sequoia Kay Hill, Erica Li, and Lara Weinstein. A qualitative exploration of the functional, social, and emotional impacts of the covid-19 pandemic on people who use drugs. *International Journal of Environmental Research and Public Health*, 19(15):9751, 2022.
- [22] Alicia Jeffers, Alisha A. Meehan, Joseph Barker, Alyson Asher, Misty P. Montgomery, Gabriella Bautista, Catherine M. Ray, Richard L. Laws, Vanessa L. Fields, Lakshmi Radhakrishnan, Seong Y. Cha, Ann Christensen, Brisnedy Dupervil, Jessica V. Verlenden, Christie H. Cassell,

- Anne Boyer, Beth DiPietro, Mary Cary, Miwa Yang, Emily Mosites, and Rachel Marcus. Impact of social isolation during the covid-19 pandemic on mental health, substance use, and homelessness: Qualitative interviews with behavioral health providers. *International Journal of Environmental Research and Public Health*, 19(19):12120, Sep 25 2022.
- [23] Centers for Disease Control and Prevention/Agency for Toxic Substances and Disease Registry. Cdc/atsdr svi data and documentation download. https://www.atsdr.cdc.gov/placeandhealth/svi/data_documentation_download.html. Accessed October 13, 2023.
- [24] Rebecca W. Knoebel and Seong J. Kim. Impact of covid-19 pandemic, social vulnerability, and opioid overdoses in chicago. *AJPM Focus*, 2(2):100086, Jun 2023.
- [25] Patrick J. Joudrey, Marynia Kolak, Qian Lin, Sara Paykin, Vanessa Anguiano, and Emily A. Wang. Assessment of community-level vulnerability and access to medications for opioid use disorder. *JAMA Network Open*, 5(4):e227028, 2022.
- [26] M Tatar, MR Faraji, K Keyes, FA Wilson, and MS Jalali. Social vulnerability predictors of drug poisoning mortality: A machine learning analysis in the united states. *Am J Addict*, 32(6):539–546, 2023.
- [27] T.C. Yang, S. Kim, S.A. Matthews, and C. Shoff. Social vulnerability and the prevalence of opioid use disorder among older medicare beneficiaries in u.s. counties. *Journal of Gerontology: Series B*, 78(12):2111–2121, December 2023.
- [28] Tianqi Chen and Carlos Guestrin. Xgboost: A scalable tree boosting system. In *Proceedings of the 22nd ACM SIGKDD International Conference on Knowledge Discovery and Data Mining*, volume 11 of *KDD '16*, page 785–794. ACM, August 2016.
- [29] Dwi Tarwidi, Sri R. Pudjaprasetya, Donny Adytia, and Muwafiq Apri. An optimized xgboost-based machine learning method for predicting wave run-up on a sloping beach. *MethodsX*, 10:102119, Mar 10 2023.
- [30] Kartik Budholiya, Shailendra Kumar Shrivastava, and Vivek Sharma. An optimized xgboost based diagnostic system for effective prediction of heart disease. *Journal of King Saud University - Computer and Information Sciences*, 34(7):4514–4523, 2022.
- [31] Andrew Moore and Melanie Bell. Xgboost, a novel explainable ai technique, in the prediction of myocardial infarction: A uk biobank cohort study. *Clinical Medicine Insights: Cardiology*, 16:11795468221133611, Nov 8 2022.
- [32] Dor Bank, Noam Koenigstein, and Raja Giryes. Autoencoders, 2021.

- [33] Pengzhi Li, Yan Pei, and Jianqiang Li. A comprehensive survey on design and application of autoencoder in deep learning. *Applied Soft Computing*, 138:110176, 2023.
- [34] Kamran Berahmand, Farhad Daneshfar, Ehsan S. Salehi, and et al. Autoencoders and their applications in machine learning: a survey. *Artificial Intelligence Review*, 57(28), 2024.
- [35] Scott Lundberg. shap.gradientexplainer. <https://shap.readthedocs.io/en/latest/generated/shap.GradientExplainer.html>, 2018. Accessed July 15, 2024.
- [36] Mukund Sundararajan, Ankur Taly, and Qiqi Yan. Axiomatic attribution for deep networks. In *Proceedings of the 34th International Conference on Machine Learning - Volume 70*, ICML'17, page 3319–3328. JMLR.org, 2017.
- [37] Scott M. Lundberg and Su-In Lee. A unified approach to interpreting model predictions. In *Proceedings of the 31st International Conference on Neural Information Processing Systems*, NIPS'17, page 4768–4777, Red Hook, NY, USA, 2017. Curran Associates Inc.
- [38] Centers for Disease Control and Prevention. Cdc wonder. <https://wonder.cdc.gov/>, 2024. Accessed August 1, 2024.
- [39] Alex Hollingsworth, Christopher J. Ruhm, and Kosali Simon. Macroeconomic conditions and opioid abuse. Working Paper 23192, National Bureau of Economic Research, Feb 2017.
- [40] UCLA Nursing. Opioid addiction crisis in united states linked to poor working conditions and unemployment. <https://nursing.ucla.edu/news/opioid-addiction-crisis-in-united-states-linked-to-poor>, 2022. Accessed September 17, 2024.
- [41] August F. Holtyn, Fabian Toegel, Michael D. Novak, and Kenneth Silverman. Factors associated with obtaining employment among opioid use disorder patients enrolled in a therapeutic workplace intervention. *Drug and Alcohol Dependence*, 226:108907, Sep 1 2021.
- [42] Timothy A. Matthews, Grace Sembajwe, Roland von Känel, and Jian Li. Associations of employment status with opioid misuse: Evidence from a nationally representative survey in the u.s. *Journal of Psychiatric Research*, 151:30–33, 2022.
- [43] Sunday Azagba, Ling Shan, Fares Qeadan, and et al. Unemployment rate, opioids misuse and other substance abuse: quasi-experimental evidence from treatment admissions data. *BMC Psychiatry*, 21(22), 2021.
- [44] ASPE Office of the Assistant Secretary for Planning and Evaluation. Economic opportunity and the opioid crisis: Geographic and economic trends. <https://aspe.hhs.gov/reports/>

economic-opportunity-opioid-crisis-geographic-economic-trends. Accessed September 17, 2024.

- [45] Mercy N. Mumba, Lori Davis, Nancy L. Smith, Tiffany Evans, and Ruben Castillo. Effects of unemployment on opioid use treatment trajectories: Impact of the covid-19 pandemic. *Journal of Addictions Nursing*, 33(3):168–171, Jul-Sep 2022.
- [46] M. Kate Wolfe, Noreen C. McDonald, and George M. Holmes. Transportation barriers to health care in the united states: Findings from the national health interview survey, 1997-2017. *American Journal of Public Health*, 110(6):815–822, Jun 2020.
- [47] Samina T. Syed, Benjamin S. Gerber, and Lisa K. Sharp. Traveling towards disease: transportation barriers to health care access. *Journal of Community Health*, 38(5):976–993, Oct 2013.
- [48] Robert Wood Johnson Foundation. More than one in five adults with limited public transit access forgo health care because of transportation barriers. <https://www.rwjf.org/en/insights/our-research/2023/04/more-than-one-in-five-adults-with-limited-public-transit-access-forgo-healthcare-because-of-transportation-barriers.html>. Accessed September 17, 2024.
- [49] CM Nguyen, G Kubiak, N Dixit, SA Young, and JR Hayes. Evaluating barriers to opioid use disorder treatment from patients’ perspectives. *PRiMER*, 8:11, 2024.
- [50] American Hospital Association. Social determinants of health series: Transportation and the role of hospitals. <https://www.aha.org/ahahret-guides/2017-11-15-social-determinants-health-series-transportation-and-role-hospitals#:~:text=Transportation%20issues%20can%20affect%20a,be%20a%20vehicle%20for%20wellness>. Accessed September 17, 2024.
- [51] Marwan Labban, Chia-Yuan Chen, Natalie Frego, and et al. Disparities in travel-related barriers to accessing health care from the 2017 national household travel survey. *JAMA Network Open*, 6(7):e2325291, 2023.
- [52] Marjorie C. Gondré-Lewis, Tomilola Abijo, and Theodore A. Gondré-Lewis. The opioid epidemic: a crisis disproportionately impacting black americans and urban communities. *Journal of Racial and Ethnic Health Disparities*, 10(4):2039–2053, Aug 2023.
- [53] RW Knoebel and SJ Kim. Impact of covid-19 pandemic, social vulnerability, and opioid overdoses in chicago. *AJPM Focus*, 2(2):100086, 2023.

- [54] Allison L. Cochran, Noreen C. McDonald, Laura Prunkl, and et al. Transportation barriers to care among frequent health care users during the covid pandemic. *BMC Public Health*, 22(1783), 2022.
- [55] Congressional Research Service. Unemployment rates during the covid-19 pandemic. Technical report, Congressional Research Service, 2021. Accessed August 1, 2024.
- [56] United States Census Bureau. Table & geography changes. <https://www.census.gov/programs-surveys/acs/technical-documentation/table-and-geography-changes.2022.html#list-tab-71983198>. Accessed October 19, 2023.
- [57] Federal Register. Change to county-equivalents in the state of connecticut. <https://www.federalregister.gov/documents/2022/06/06/2022-12063/change-to-county-equivalents-in-the-state-of-connecticut>. Accessed September 1, 2024.
- [58] CDC National Center for Health Statistics. Icd-10. https://www.cdc.gov/nchs/icd/icd-10/index.html#cdc_generic_section_3-icd-10, 2024. Accessed August 1, 2023.
- [59] CDC National Center for Health Statistics. Provisional drug overdose death counts. <https://www.cdc.gov/nchs/nvss/vsrr/drug-overdose-data.htm>, 2024. Accessed August 1, 2023.
- [60] Chandra Tiwari, Kirsten Beyer, and Gerard Rushton. The impact of data suppression on local mortality rates: the case of cdc wonder. *American Journal of Public Health*, 104(8):1386–1388, Aug 2014.
- [61] PySAL Development Team. Tobler github repository. <https://github.com/pysal/tobler>, 2023. Accessed August 30, 2024.
- [62] United States Census Bureau. Data collection error in rio arriba county, nm. <https://www.census.gov/programs-surveys/acs/technical-documentation/errata/125.html>. Accessed February 15, 2024.
- [63] G Erion, JD Janizek, P Sturmfels, S Lundberg, and SI Lee. Improving performance of deep learning models with axiomatic attribution priors and expected gradients, 2020.

Figures and Tables

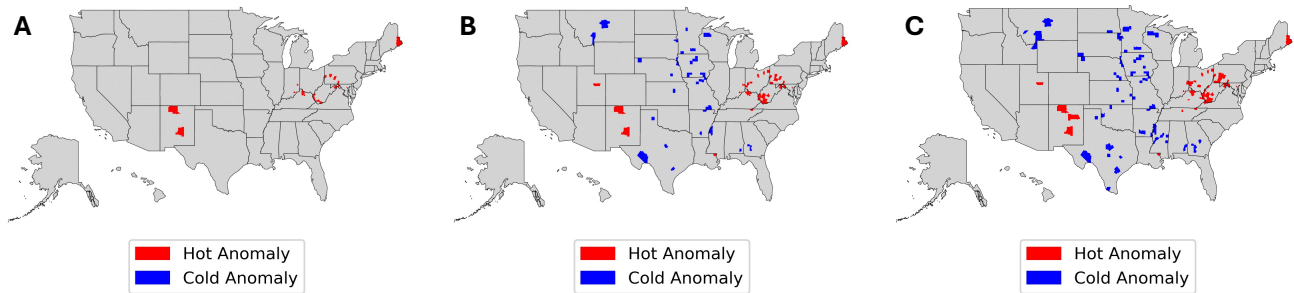


Figure 1: A) 2016 anomaly map using 1% tails. B) 2016 anomaly map using 2% tails. C) 2016 anomaly map using 3% tails. A 1% threshold produced no cold anomalies, while a 2% threshold provided the smallest bound that yielded cold anomalies. Increasing the threshold to 3% further raised the number of anomalies in both categories. Figures are best viewed in color.

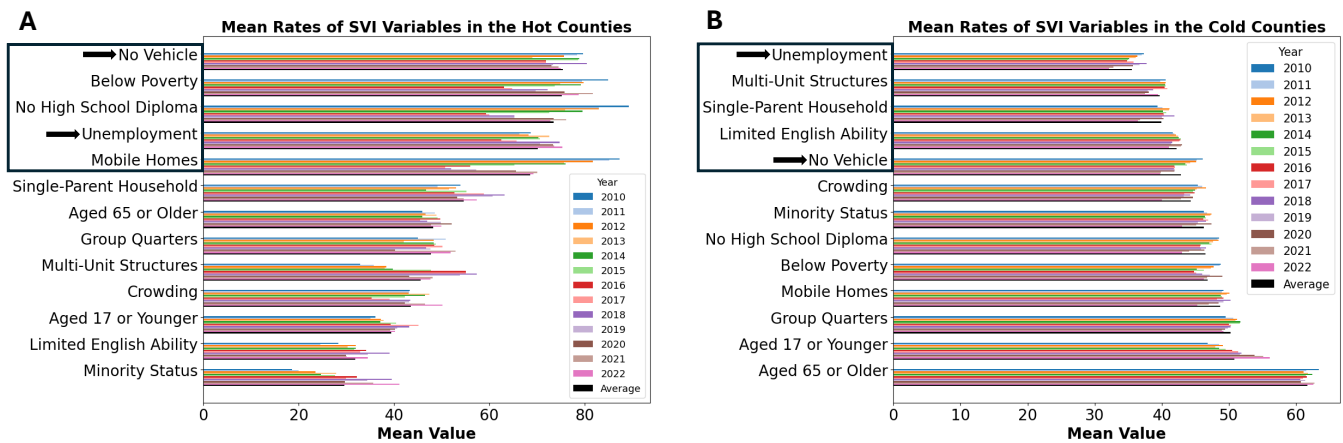


Figure 2: A) Hot anomaly summary, where features are ranked from highest average mean rate down to lowest. B) Cold anomaly summary, where features are ranked from lowest average mean rate down to highest. In both plots, each feature's yearly mean rates are displayed using colored bars, while the black bars showcase each feature's average mean rate across all years in the study. Figures are best viewed in color.

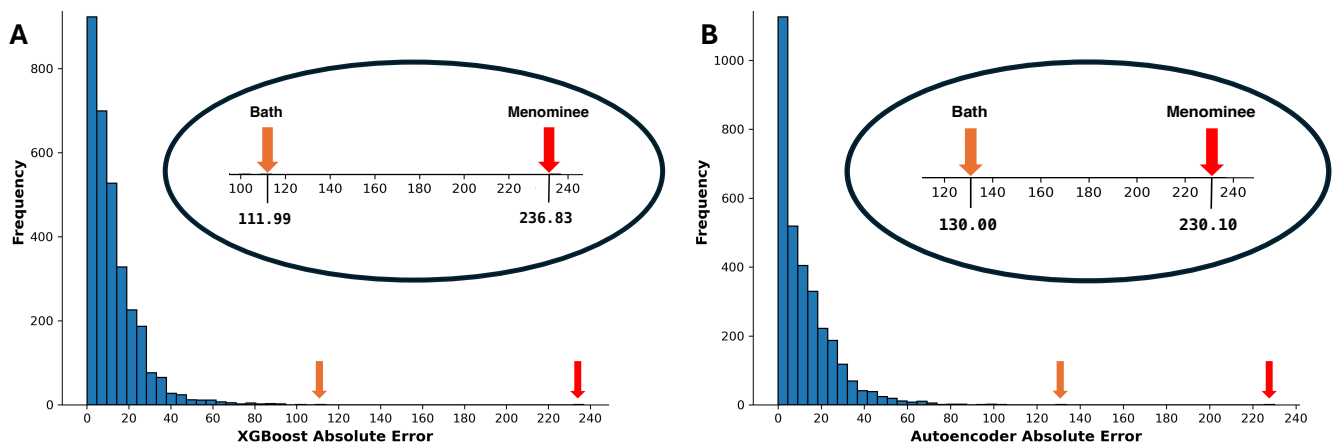


Figure 3: A) Histogram displaying the distribution of XGBoosts’s absolute errors for the 2022 mortality rate predictions. B) Histogram displaying the distribution of the autoencoder’s absolute errors for the 2022 mortality rate predictions. In both plots, the error stemming from Menominee County, Wisconsin, is indicated by the red arrow, while the error stemming from Bath County, Kentucky, is indicated by the orange arrow. Figures are best viewed in color.

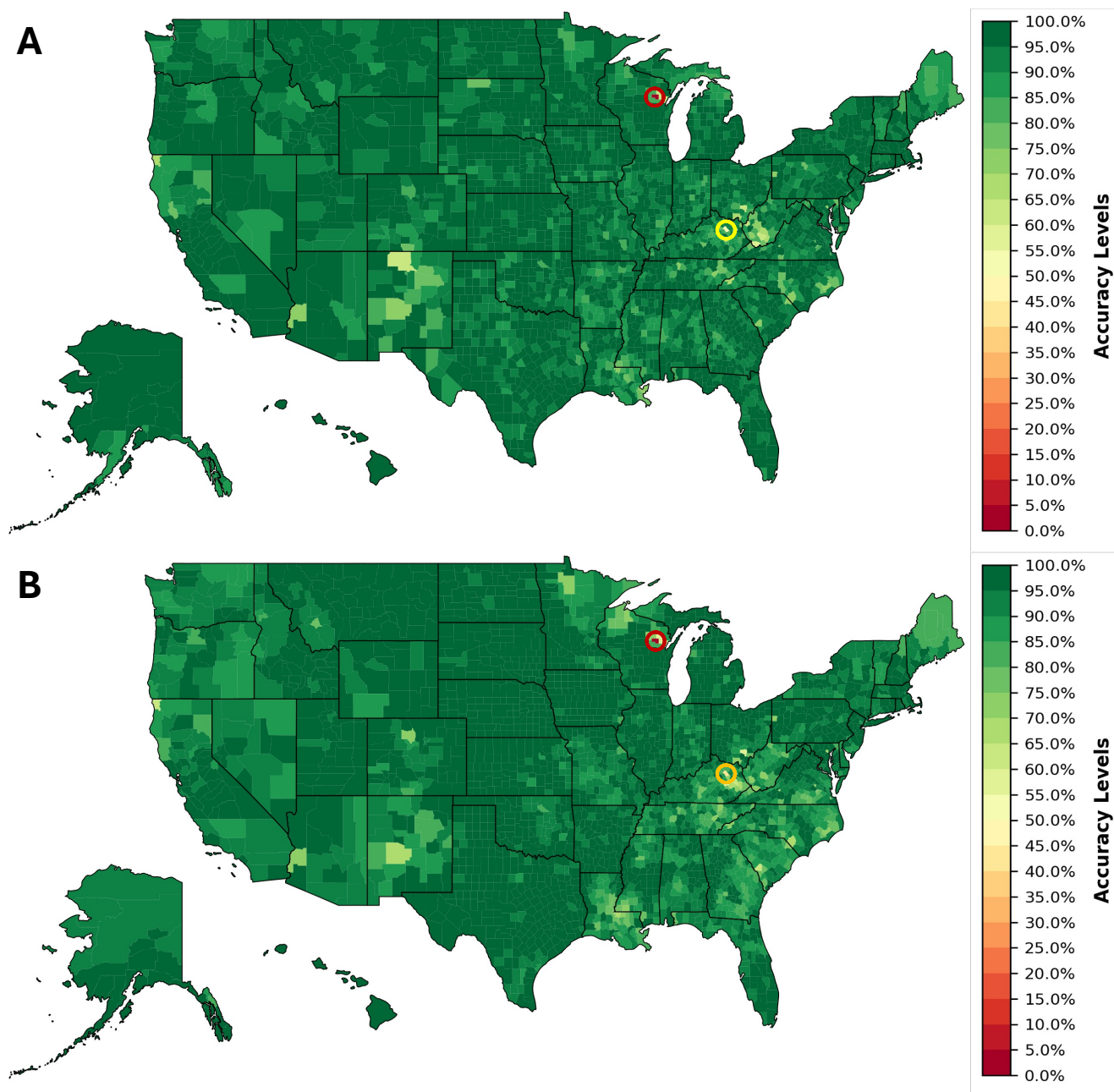


Figure 4: A) Accuracy map for XGBoost’s 2022 mortality rate predictions. B) Accuracy map for the autoencoder’s 2022 mortality rate predictions. Both maps are color-coded to represent increasing intervals of accuracy by 5%, starting from dark red for the least accurate predictions, and progressing to dark green for the most accurate predictions. In both plots, Menominee County, Wisconsin, which had the largest 2022 error for both models, is shaded in the darkest red. To make it easier to locate, this county is also circled in the same color. Bath County, Kentucky, is shaded in orange on the autoencoder’s accuracy map and in yellow on XGBoost’s map, highlighting that the autoencoder had a higher error here than XGBoost. This county has also been circled in its respective color for easier visual identification. Figures are best viewed in color.

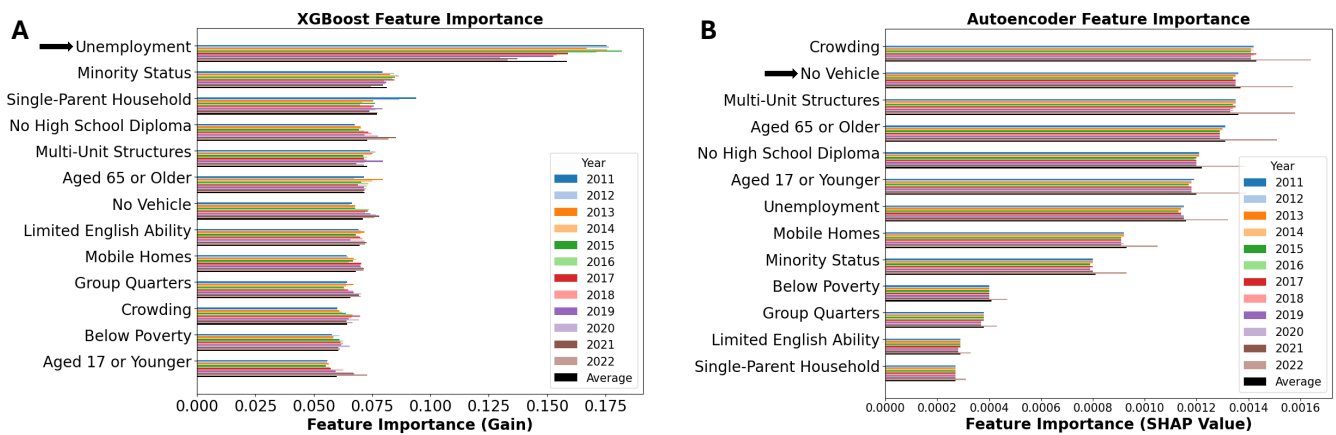


Figure 5: A) XGBoost feature importance summary. B) Autoencoder feature importance summary. Both plots display each feature’s yearly importance scores with colored bars, while black bars represent the average importance scores across all years. Features are ranked by their average importance, from highest to lowest in both plots. Figures are best viewed in color.

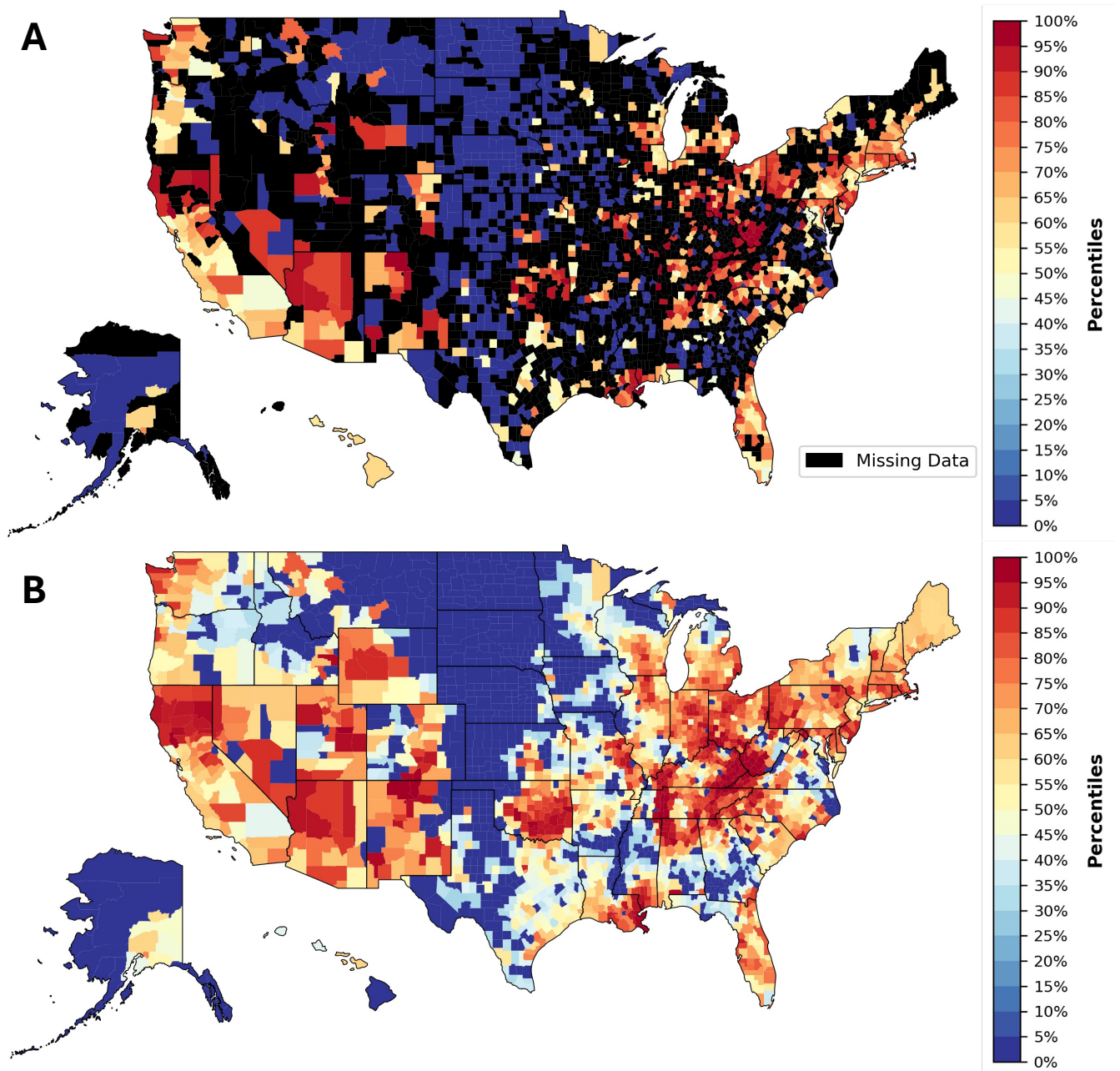


Figure 6: A) 2013 missing data map. B) 2013 interpolated data map. Each map is colored by percentiles from the respective empirical distributions. Figures are best viewed in color.

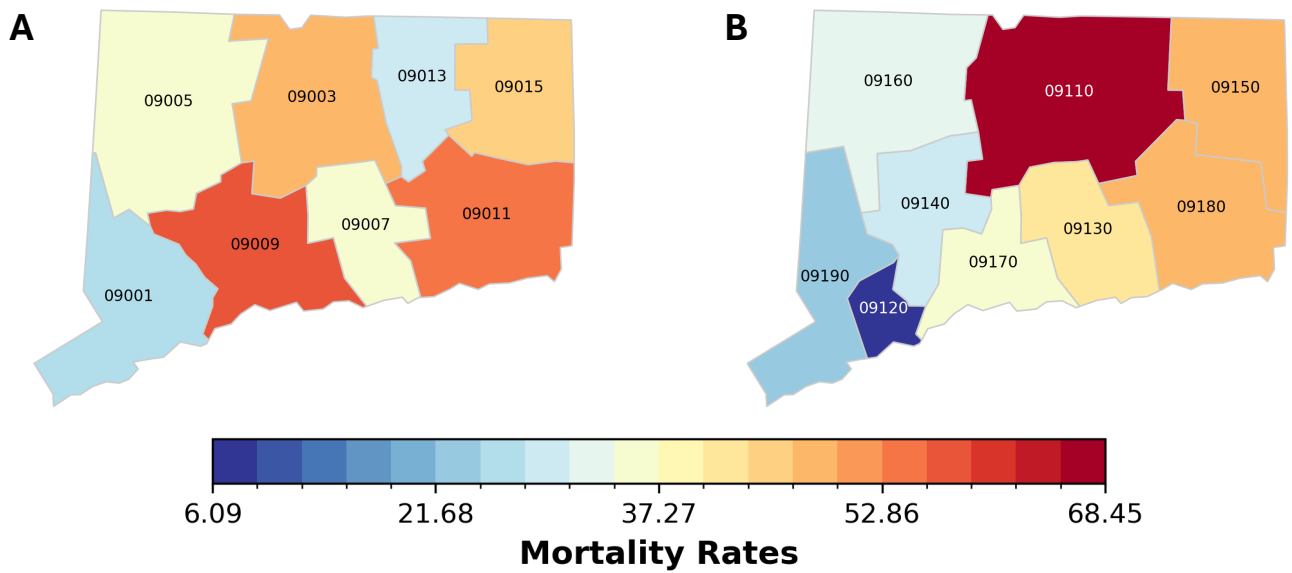


Figure 7: A) 2021 mortality rates for the old (pre-2022) Connecticut county structure. B) 2021 mortality rates for the new (2022) Connecticut county structure. The color scales for both maps are normalized to the minimum and maximum 2021 mortality rates across both county structures. The minimum 2021 mortality rate is 6.09, shown in the darkest blue, while the maximum rate is 68.45, shown in the darkest red. Figures are best viewed in color.

Theme	Feature	Definition
Socioeconomic Status	Below poverty	Percentile percentage of persons below poverty estimate
	Unemployment	Percentile percentage of civilian (age 16+) unemployed estimate
	No high school diploma	Percentile percentage of persons with no high school diploma (age 25+) estimate
Household Characteristics	Age 65 and older	Percentile percentage of persons aged 65 and older estimate
	Age 17 and younger	Percentile percentage of persons aged 17 and younger estimate
	Single-parent households	Percentile percentage of single-parent households with children under 18 estimate
	Limited English ability	Percentile percentage of persons (age 5+) who speak English “less than well” estimate
Racial and Ethnic Minority Status	Minority Status	Percentile percentage minority (Hispanic or Latino (of any race); Black and African American, Not Hispanic or Latino; American Indian and Alaska Native, Not Hispanic or Latino; Asian, Not Hispanic or Latino; Native Hawaiian and Other Pacific Islander, Not Hispanic or Latino; Two or More Races, Not Hispanic or Latino; Other Races, Not Hispanic or Latino) estimate
Housing Type and Transportation	Multi-unit structures	Percentile percentage of housing structures with 10 or more units estimate
	Mobile homes	Percentile percentage mobile homes estimate
	Crowding	Percentile percentage of households with more people than rooms estimate
	No vehicle	Percentile percentage of households with no vehicle available estimate
	Group quarters	Percentile percentage of persons in group quarters estimate (e.g., correctional institutions, nursing homes)

Table 1: Definitions of the social vulnerability features utilized in this study.

Year	Avg Error		Max Error		Avg Accuracy	
	XGB	AE	XGB	AE	XGB	AE
2011	5.79	4.07	100.18	72.41	94.22%	94.39%
2012	5.67	4.08	72.14	72.88	92.14%	94.40%
2013	5.86	3.97	78.39	55.25	92.52%	92.82%
2014	6.43	3.56	87.57	59.17	92.66%	93.98%
2015	6.65	3.26	112.40	68.05	94.09%	95.22%
2016	7.83	4.66	107.68	100.36	92.73%	95.36%
2017	8.34	4.15	126.24	72.20	93.39%	94.25%
2018	8.18	3.94	98.80	48.67	91.72%	91.91%
2019	8.43	4.02	97.56	60.61	91.36%	93.36%
2020	10.78	7.35	136.70	92.04	92.11%	92.02%
2021	13.84	11.60	161.62	184.12	92.06%	93.70%
2022	12.44	12.37	236.83	230.10	94.75%	94.62%

Table 2: Efficacy metric summary for both the XGBoost (XGB) and autoencoder (AE) models. For each county, the error is measured as the absolute residual, while the accuracy is calculated as the county’s error normalized by the highest observed error nationwide.